Photochemical & Photobiological Sciences

ROYAL SOCIETY OF CHEMISTRY

PAPER

View Article Online
View Journal | View Issue

Cite this: *Photochem. Photobiol. Sci.*, 2020, **19**, 1538

Theoretical determination of two-photon absorption in biologically relevant pterin derivatives

Thomas Malcomson *[a] and Martin J. Paterson [b]

Received 31st July 2020,
Accepted 23rd September 2020

DOI: 10.1039/d0pp00255k

rsc.li/pps

Given the prevalence of fluorescence spectroscopy in biological systems, and the prevalence of pterin derivatives throughout biological systems, presented here is an assessment of the two-photon absorption spectroscopy as it applies to a range of the most commonly studied pterin derivatives. QR-CAMB3LYP//ccpVTZ calculations suggest that the use of two-photon spectroscopic methods would enable a more capable differentiation between closely related derivatives in comparison to the one-photon spectra, which show minimal qualitative deviation. Study of short tail derivatives shows that, in most cases, two-photon accessible states solely involve the π^* LUMO as the particle orbital, with biopterin, neopterin, and 6-(hydroxymethyl)pterin presenting exceptional potential for targetting. Investigation of derivatives in which the tail contains an aromatic ring resulted in the observation of a series of two-photon accessible states involving charge transfer from the tail to the pterin moiety, the cross sections of which are highly dependent on the adoption of a planar geometry. The observation of these states presents a novel method for tracking the substitution of biologically important molecules such as folic acid and 5-methenyltetrahydrofolylpolyglutamate.

1. Introduction

The pterin family of molecules are defined as low weight heterocycles derived from the substitution of a pteridine ring with a amino (–NH_2) and carbonyl (–C=O) groups at the C2 and C4 ring positions, respectively. Although both nitrogen and oxygen centres are possible targets for nucleophilic attack, the central pterin moiety (Fig. 1) is more commonly functionalised through the addition of substituent groups to the C6 position, located on the pyrazine ring.[1]

Behaving as weak acids in aqueous solution, pterins form a dominant equilibrium at pH > 5 consisting of the acidic (amino) and basic (phenolate) form (Fig. 1)[2] with the pK_a of this equilibrium, centred around the protonation state of the N3 proton, is *ca.* 8 [3] for the derivatives shown in Table 1. The pK_a of other pterin-based protons, specifically those located on the N1 amino group, are <2.[2]

Throughout this work, for the ease of discussion, the acidic and basic forms of each molecule, when appropriate, will be marked by a subscript letter ($\mathbf{PT_a}$ and $\mathbf{PT_b}$ representing the acidic and basic forms of the unsubstituted pterin moiety, respectively).

Pterins, and their derivatives, are found throughout biology. While their oxidised states have been found extensive medical use, acting as markers for a range of conditions, including: vitiligo,[4] cardiovascular diseases,[5,6] along with activation of immune responses and synthesis of neurotransmitters,[7,8] pterins are also found naturally within human biology; folic acid (vit B9) acts as a coenzyme during reactions involved in the synthesis of both purine and pyridine DNA bases.[9] Biopterin (**BPT**) has been found taking the role of a coenzyme in hydroxylation reactions in the metabolism of both amino acids and nitric oxide[10,11] while neopterin (**NPT**), a **BPT** metabolite, is synthesised predominantly in activated macrophages with high levels of **NPT** found in response to

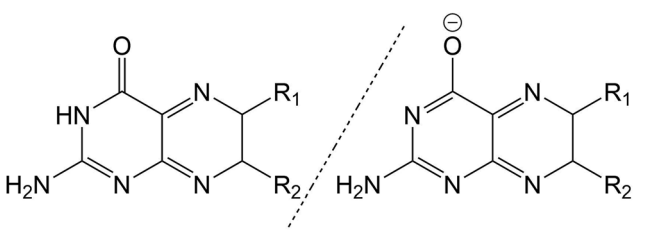

Fig. 1 Structure of pterin moiety in its acidic (left) and basic (right) states.

[a]*Department of Chemistry, Lancaster University, Lancaster, LA1 4YB, UK. E-mail: t.malcomson@lancaster.ac.uk*
[b]*School of Engineering and Physical Sciences, Heriot-Watt University, Edinburgh, EH14 4AS, UK. E-mail: m.j.paterson@hw.ac.uk*

infections caused by viruses, parasites and intracellular bacteria.[12–17] Despite the role of 5,10-methenyltetrahydrofolylpolyglutamate, a derivative of folic acid (**FA**), in DNA repair as a light-harvesting antenna in DNA photolyases,[18–20] oxidised pterins have also been shown to cause photo-activated DNA damage when exposed to UV light.[21–25]

The ability of pterins to produce singlet oxygen ($O_2(^1\Delta_g)$, denoted as $^1O_2$ for simplicity)[26,27] has garnered particular interest due to its role in photodynamic therapy (PDT).[28,29] This metastable state of molecular oxygen, produced primarily through photosensitisation, is significantly more reactive than the triplet ground state ($O_2(^3\sum^-_g)$). The pterin-induced production of $^1O_2$ is brought about due to ready access of the pterin molecules to a triplet excited state through intersystem crossing,[30,31] enabling a spin crossover with the $^3O_2$ state of molecular oxygen in place of the commonly observed pterin phosphorescence.[26,32]

However, the ideal wavelength of light needed to achieve the production of singlet oxygen is in the region of 350 nm which has a very poor tissue penetration value as, due to scattering from the cell nuclei, mitochondria, the Golgi apparatus and the cellular surface itself,[33,34] the optical penetration of biological tissue is low, usually measured in millimetres.[35] Tissue penetration varies greatly depending on the tissue type and the wavelength used, with longer wavelengths appearing to penetrate to a greater degree, with Stolik *et al.* reporting a depth of 4.23 ± 0.03 mm.[35]

While $^1O_2$ has been shown to be a dominant mediator of phototoxic effects, it is a short lived species (<200 ns *in vitro*).[36–38] As a result of this, the diffusion of $^1O_2$ is limited to short distances (≈1 μm),[39–41] limiting the cytotoxicity to immediate area around the production location. The low diffusion of $^1O_2$ through a biological medium does, however, limit its use as a photoactivated target due to the tissue depth penetration of the UV light required to excite the pterin molecules.[42,43] This limitation can be reduced through with the use of near IR light (λ = 600–100 nm) *via* two-photon absorption (TPA) which, in addition to the increased tissue penetration of higher wavelength light, increases the spatial resolution of photo-activation.

Despite this promising avenue of investigation, coupled with the pterin molecule acting as a design precursor for a number of fluorescent DNA analogues[44,45] and the otherwise extensive detail to which the photochemistry of these molecules has been investigated,[26,27,30–32,46] studies of the potential two-photon activation of pterin derivatives is poorly explored. In response to this, we present here a study of the susceptibility of a series of well studied, biochemically relevant pterin derivatives to two-photon activation through the use of quadratic response (QR) density functional theory (DFT) methodologies. The use of these methodologies for the accurate determination of TPA spectra has been well established across a range of molecules of both biological and photochemical importance.[47–53]

The structures studied here are presented in three groups: the first involves small functional group alterations to the core pterin moiety at the C6 (Table 1); the second involves the inclusion of extended side chains (Fig. 2) centred around the folic acid structure (**FA**); the final grouping of structures (Fig. 3), centred around 5-methenyltetrahydrofolylpolyglutamate (**MTHFG**), denote a series of biological, pterin derived, cofactors. These groups are selected to provide a thorough representation of the TPA viability of

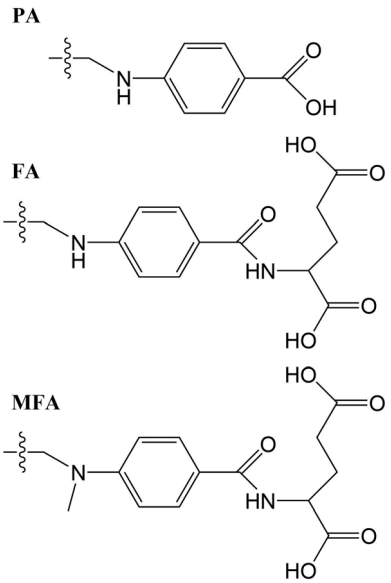

Fig. 2 Extended R-groups for pterin derivatives.

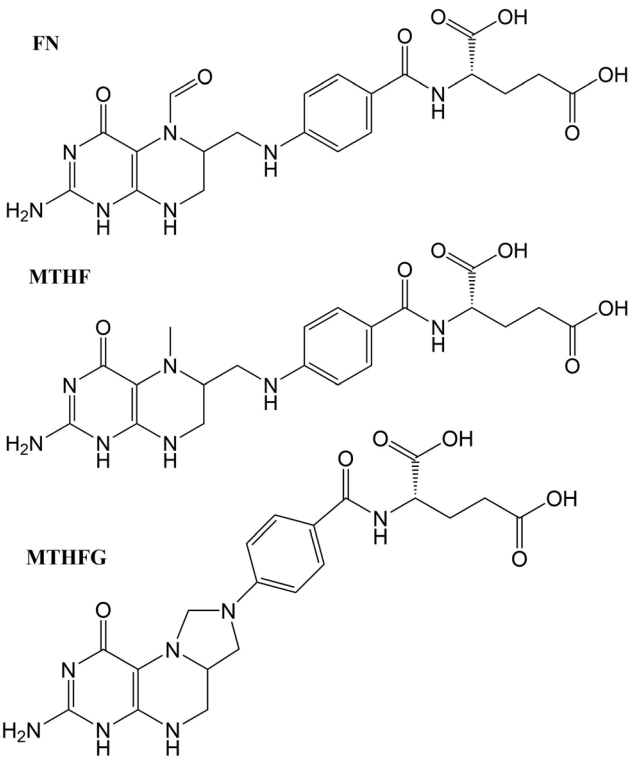

Fig. 3 One-photon absorption spectra of pterin derivatives in their acidic state.

Table 1 Excited state energies (eV) and two-photon cross sections (GM) of the unsubstituted pterin structure

	Acid		Base	
State	Energy	σ^{TP}	Energy	σ^{TP}
1	3.8466	0.000	3.6378	0.000
2	4.3353	0.058	3.7888	0.077
3	4.7731	0.001	4.2833	0.000
4	4.9175	0.000	4.6724	0.026
5	5.0735	0.164	4.7912	0.002
6	5.4911	0.006	4.9873	0.003
7	6.0768	0.006	5.3212	0.286
8	6.2832	0.008	5.6911	0.007
9	6.3615	0.260	5.8665	0.010
10	6.5497	0.332	5.9080	0.002

Table 2 R-group variation of investigated pterins

Abbrv.	Name	R_1	R_2
PT	Pterin	–H	H
BPT	Biopterin	$-(CHOH)_2CH_3$	H
CPT	6-Carboxypterin	–COOH	H
DPT	6,7-Dimethylpterin	$-CH_3$	$-CH_3$
FPT	6-Formylpterin	–CHO	H
HPT	6-(Hydroxymethyl)pterin	$-CH_2OH$	H
MPT	6-Methylpterin	$-CH_3$	H
NPT	Neopterin	$-(CHOH)_2CH_2OH$	H
RPT	Rhamnopterin	$-(CHOH)_3CH_3$	H
PA	Pteroic acid	[a]	H
FA	Folic acid	[a]	H
MFA	10-Methylfolic acid	[a]	H
FN	Folinic acid	[b]	H
MTHF	L-5-Methyltetrahydrofolate	[b]	H
MTHFG	5,10-Methenyltetrahydrofolyl-polyglutamate	[b]	H

[a] R_1 groups for pterin derivatives with extended side chains are shown in Fig. 2. [b] Structures for derivatives involving biological alterations to the central pterin moiety are shown in Fig. 3.

the pterin family of molecules throughout their biological function.

The successful determination of the TPA spectra for these derivatives opens up a number of avenues for further investigation, from TPA access to the triplet states of these derivatives and their potential for $^1O_2$ production, to the ability to track the presence of specific derivatives despite the one-photon absorption (OPA) spectra of these structures showing little qualitative variation.

2. Theoretical methods

Geometry optimisations and TD-DFT calculations were carried out with the Gaussian16 software package.[54,55] Optimisations utilised the B3LYP functional[56–60] with Grimme's D3 dispersion[61] and Becke–Johnson dampening[62–65] along with the 6-311G** basis set[66] with the determination of structural minima conducted through frequency analysis and noted by the presence of only positive curvature; the use of this model chemistry has been well established for giving appropriate geometry determinations for molecules of this type.[17,67–71] TD-DFT data was determined using a series of DFT functionals, namely: CAM-B3LYP,[72] B3LYP,[56–60] BP86[73,74] and PBE0,[75] each with the Dunning cc-pVTZ basis.[76] CAM-B3LYP values are reported here due to their agreement with the UV-Vis spectra of folic acid,[77] as well as its robust performance on similar organic molecules.[78,79] The use of CAM-B3LYP for the QR-DFT calculations has been well established in providing high accuracy values for similar systems.[47–49,80–83]

Two-photon cross sections (σ^{TP}), as defined through QR-DFT implemented in Dalton,[84] are determined by:

$$\sigma^{TP} = \frac{8\pi^3\alpha^2\hbar}{e^4}E^2\delta^{TP} \quad (1)$$

where:

$$E = \frac{\omega}{\Gamma} \quad (2)$$

such that ω is the photon energy in eV and Γ is a broadening factor of 0.1 eV, α is the fine line constant, and the transition strength (δ^{TP}) is given by:[80]

$$\delta^{TP} = F\delta^F + G\delta^G + H\delta^H \quad (3)$$

in which F, G, and H vary depending on the polarisation of light use; under parallel linearly polarised light, $F = G = H = 2$. In addition, each component ($\delta^F/\delta^G/\delta^H$) takes the form:

$$\delta^F = \frac{1}{30}\sum_{\alpha,\beta} S_{\alpha\alpha}S_{\beta\beta} \quad (4)$$

$$\delta^G = \frac{1}{30}\sum_{\alpha,\beta} S_{\alpha\beta}S_{\alpha\beta} \quad (5)$$

$$\delta^H = \frac{1}{30}\sum_{\alpha,\beta} S_{\alpha\beta}S_{\beta\alpha} \quad (6)$$

where α and β are the components of the dipole operator such that α, $\beta = x, y, z$, and the sums contained within each term run over combinations of these components for the operators acting between the ground ($|0\rangle$), intermediate ($|i\rangle$), and final ($|f\rangle$) states, such that:

$$S_{\alpha,\beta} = \sum_i \frac{\langle 0|\mu^\alpha|i\rangle\langle i|\mu^\beta f\rangle}{\omega_i - \frac{\omega_f}{2}} + \frac{\langle 0|\mu^\beta|i|\rangle\langle i|\mu^\alpha|f\rangle}{\omega_i - \frac{\omega_f}{2}} \quad (7)$$

where ω_i is the transition frequency to the intermediate (virtual) state, and ω_f is the transition frequency for the final state; *i.e.* the state in question.

3. Results and discussion

3.1. Acid *vs.* base susceptibility for one- and two-photon absorption

Across pterins involving the addition of small, non-aromatic substituents, a single dominant (defined here as a state with a

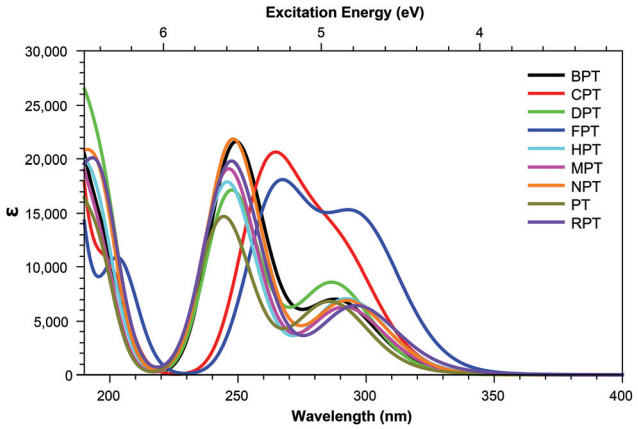

Fig. 4 One-photon absorption spectra of pterin derivatives in their acidic state.

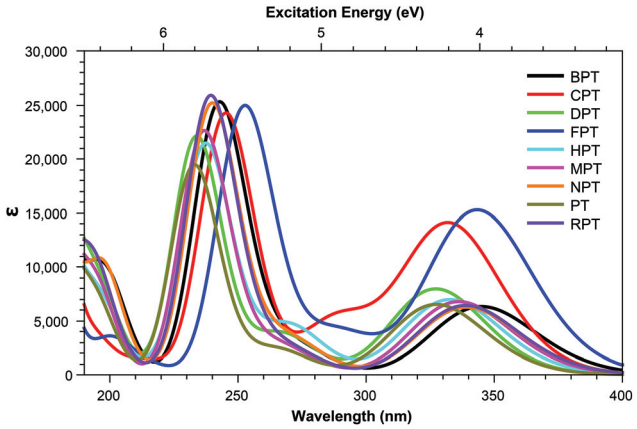

Fig. 5 One-photon absorption spectra of pterin derivatives in their base form.

cross section >1.0 GM) can be observed in the acid form; this state can be seen moving to a lower energy in the basic form, a trend contrary to that observed in the the OPA spectra (Fig. 4 and 5). When considering the OPA spectra of the base forms of small-tail derivatives the dominant transitions are to S_2 and S_7 for the peaks at approx. 340 nm and 240 nm, respectively. In the two-photon spectra, these states remain accessible, with cross-sections for S_2 (S_1 for **NPT$_b$**) ranging from 0.1–1.3 GM while S_7 is seen to possess more substantial cross-section values, ranging from 4.1–10.7 GM. In contrast to the base spectra, the spectra for the acidic form (Table 4) is less predictable. While S_2 is still accessible for most derivatives (with the exception of **FPT$_a$** & **HPT$_a$**), the state corresponding to the higher energy peak is more variable, with dominant transitions to states S_5, S_8, S_9, or S_{10} observed, depending on the derivative. However, similar to what is observed in the base form, states showing strong oscillator strengths in the OPA spectra remain accessible in the TPA spectra with ranges for S_2 from 0.19–1.1 GM and, with the exception of **FPT$_a$**, a range of 4.6–9.5 GM for states found in the region of the higher energy OPA peak. This maintained susceptibility when moving from one- to two-photon absorption allows for the continued photoreactivity of each pterin derivative to be monitored in a similar manner to those of modern fluorescent spectroscopy methods, while also utilising of the benefits of TPA spectroscopy, including: greater spectroscopic resolution and tissue depth penetration, as well as reduced potential for unnecessary tissue damage when targetting the higher energy peak, which would otherwise necessitate the use of a high energy UV light source.

The inclusion of substituents containing an aromatic group, such as those highlighted in Fig. 2, results in similar trends to those of the smaller, non-aromatic, substituents in that large cross-section values relating to the higher energy peak of the OPA spectra (Fig. 8 and 9) remaining accessible in both acid and base forms, while the high values observed in lower states are quenching when adopting the basic form (Tables 5 and 6).

Overall, despite the structures with tails inclusive of aromatic groups showing greater similarity between the acid and base forms than their small tail counterparts, the TPA spectra mimics the properties of the OPA spectra closely with similar shifts in state energies. The TPA differs from the OPA spectra, however, in the emergence of additional accessible states upon adoption of the base form of a number of derivatives; this, adding additional possibilities for the identification of the form present *in vitro* through the use of fluorescent spectroscopy.

3.2. Effects of non-aromatic substituents

Tables 3 shows that, regardless of whether in their acidic or basic form, the unsubstituted pterin molecule (**PT**) exhibits no significant two-photon cross section (σ^{TP}) with the highest value of 0.332 GM for S_{10} of **PT$_a$**, lying at 6.55 eV. Despite this low potential, the addition of a substituent at the C6 position results in a 10-fold increase in the cross sections for the majority of substituents shown across Tables 2 and 4; the only structure that does not present an accessible state with a cross section of greater than 1 GM is **FPT$_a$**. In contrast to the OPA spectra (Fig. 4 and 5), which show a significant amount of overlap in terms of bright regions, the TPA spectra shows enhanced resolution with accessible states separating; this would suggest that the use of TPA spectroscopy could allow for the identification of a specific derivative even when other derivatives are present. An example of this can be seen in the **NPT$_a$** derivative which, despite showing a near equivalent OPA spectra to most other derivatives (Fig. 4), shows a TPA accessible state at 5.42 eV for which the only other accessible states in the region is the 5.32 eV S_6 state of **RPT$_a$** and the 5.30 eV S_7 state of **DPT$_b$**, both of which present a cross section of less than half the size (4.78 GM (Table 2) and 4.18 GM (Table 4), respectively). A similar pattern can be observed with the S_7 state of **BPT$_b$** at 5.05 eV and S_8 state of **HPT$_b$** at 5.61 eV which presents the highest cross-section of all small-tail derivatives at 39.60 GM.

With the exception of **FPT**, which consists of a predominantly HOMO → LUMO+1 transition, the dominant state for each derivative (Tables 2 and 4) involve the same π–π* tran-

Table 3 State energies (eV) and two-photon cross sections (GM) of pterin derivatives in their acidic form

	BPT		CPT		DPT		FPT		HPT		MPT		NPT		RPT	
State	E	σ^{TP}	E	σ^{TP}	E	σ^{TP}	E	σ^{TP}	E	σ^{TP}	E	σ^{TP}	E	σ^{TP}	E	σ^{TP}
1	3.89	0.007	3.80	0.000	3.99	0.002	3.46	0.000	3.85	0.000	3.87	0.001	4.00	0.014	3.82	0.009
2	4.29	0.646	4.28	0.186	4.32	0.616	3.80	0.000	4.24	0.057	4.25	0.489	4.24	0.497	4.19	0.723
3	4.75	0.031	4.39	0.002	4.85	0.037	4.16	0.343	4.83	0.002	4.83	0.024	4.92	0.120	4.83	0.115
4	4.95	0.099	4.72	0.613	5.00	1.070	4.38	0.002	4.96	0.002	4.95	0.024	5.00	1.150	4.96	0.190
5	4.98	3.010	4.85	0.134	5.01	1.220	4.67	0.660	5.05	0.128	5.03	2.030	5.03	0.037	5.02	0.869
6	5.47	0.181	4.94	0.015	5.52	0.049	4.76	0.002	5.46	0.071	5.48	0.680	5.42	10.900	5.32	4.780
7	6.06	0.307	5.41	0.050	6.13	0.060	5.22	0.027	6.11	0.099	6.14	0.060	5.50	0.663	5.50	0.122
8	6.22	6.630	5.77	0.076	6.28	9.460	5.58	0.036	6.24	8.920	6.30	0.321	6.10	0.101	6.11	0.830
9	6.32	4.640	6.09	0.091	6.38	0.598	5.74	0.114	6.29	0.273	6.34	4.700	6.31	4.650	6.21	3.000
10	6.42	0.282	6.21	9.490	6.43	5.140	6.07	0.659	6.44	0.723	6.46	5.990	6.35	2.740	6.25	3.370

Table 4 State energies (eV) and two-photon cross sections (GM) of pterin derivatives in their base form

	BPT		CPT		DPT		FPT		HPT		MPT		NPT		RPT	
State	E	σ^{TP}	E	σ^{TP}	E	σ^{TP}	E	σ^{TP}	E	σ^{TP}	E	σ^{TP}	E	σ^{TP}	E	σ^{TP}
1	3.57	0.424	3.45	0.001	3.75	0.116	3.30	0.001	3.64	0.003	3.60	0.022	3.65	1.070	3.64	0.134
2	3.61	0.859	3.73	0.268	3.79	1.330	3.61	0.327	3.73	0.107	3.69	1.340	3.68	0.157	3.66	1.280
3	4.26	0.026	4.10	0.000	4.37	0.009	3.83	0.001	4.30	0.001	4.26	0.011	4.36	0.013	4.31	0.007
4	4.56	0.701	4.28	0.326	4.64	0.882	4.06	0.001	4.59	0.232	4.65	0.703	4.60	0.772	4.62	0.758
5	4.76	0.071	4.31	0.029	4.85	0.026	4.28	0.110	4.78	0.003	4.83	0.532	4.82	0.062	4.81	0.055
6	4.90	0.021	4.81	0.123	5.07	0.040	4.29	2.730	4.96	0.042	4.97	0.032	4.95	0.014	4.96	0.058
7	5.11	4.590	5.05	10.700	5.30	4.180	4.77	0.139	5.22	9.770	5.24	4.440	5.17	4.030	5.18	5.440
8	5.71	0.566	5.28	0.016	5.63	0.848	4.91	0.001	5.61	39.600	5.67	0.078	5.78	0.200	5.74	0.110
9	5.85	0.178	5.39	0.048	5.69	0.064	5.30	0.040	5.66	0.068	5.90	0.209	5.89	0.214	5.75	20.200
10	5.92	0.100	5.44	0.055	5.87	0.151	5.43	0.102	5.85	0.048	5.94	0.035	5.91	1.800	5.93	0.104

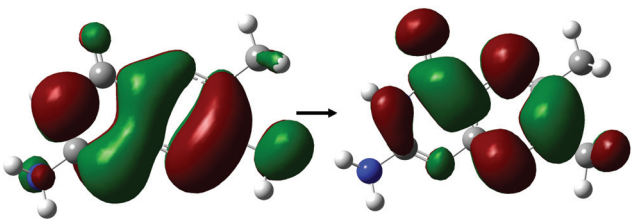

Fig. 6 Dominant orbital transition describing the two-photon accessible state showing high cross sections across small tail pterin derivatives, as shown for the $\mathbf{DPT_a}$ structure.

sition (Fig. 6); the presence of this state represents a transition that, while energetically effected by the tail, remains accessible.

3.3. Effect of aromatic substituents

Derivatives including an aromatic moiety in the tail (Fig. 2) show similar spectral features to that of the small tail derivatives; showing a small number of accessible states with high cross sectional values spread throughout a manifold of states that show low to moderate accessibility. The differences between these derivatives and those containing small tails becomes evident when assessing the OPA spectra (Fig. 8 and 9), in which the stereotypical shoulder shown at the 300–350 nm range remains present and at a similar intensity to that of the small tail derivatives while the larger peak seen at ≈250 nm presents a significant increase in intensity.

In contrast, the TPA spectra appears to consist of states which can be characterised in one of three ways: charge transfer states, in which density moves from the aromatic ring of the tail to the pterin moiety; or π–π* states isolated to either the pterin moiety or the tail; representations of these states are shown in Fig. 7.

For the acid form (Table 5) shows that, for both $\mathbf{PA_a}$ and $\mathbf{FA_a}$, the S_1 state situated at 3.87 and 3.84 eV, respectively, is significantly more accessible than its OPA counterpart with respect to the rest of their corresponding spectra; this state is, notably, quenched upon adopting the base form (Table 6). Unlike the S_1 state, the second TPA accessible region, represented by S_5 of each derivative in the acid form remains relatively intact in the base form with an average shift from 4.80 eV to 4.40 eV (noting that the TPA accessible S_5 state of the acid form (Table 5) migrates to the S_4 position when in the base form (Table 6)).

The S_1 state of these derivatives, which show a large cross sectional value for both $\mathbf{PA_a}$ and $\mathbf{FA_a}$ (Table 5), is characterised by a charge transfer from the π HOMO, isolated on the pterin moiety, to the π* LUMO on the aromatic ring of the tail, as shown in Fig. 7. The methylation of the bridging nitrogen in **MFA** (Fig. 2), which causes the structure to fold so that the phenyl ring of the tail is orientated perpendicular to the plane

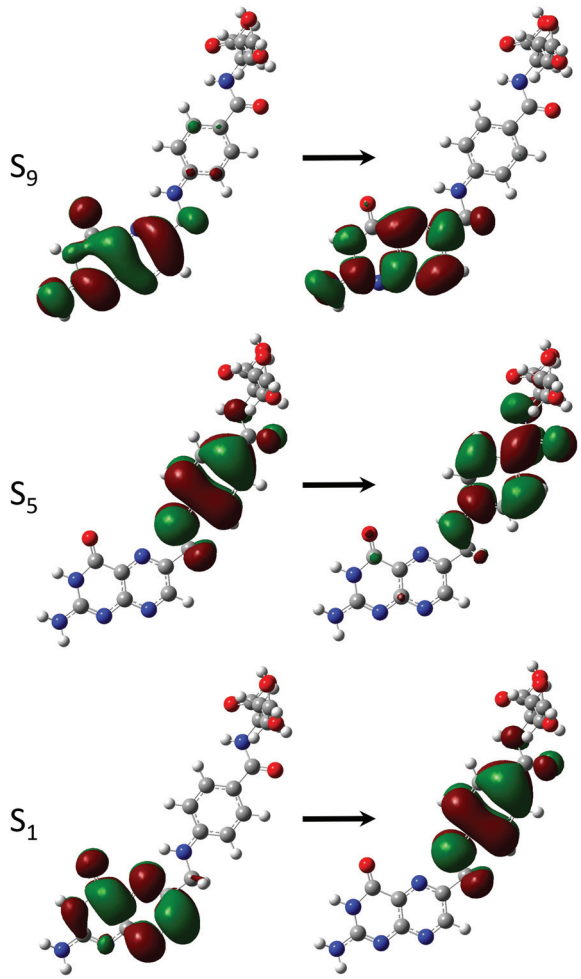

Fig. 7 Dominant orbital transitions describing the two-photon accessible states showing high cross sections in FA_a as a representation of those excitations that are two-photon accessible within derivatives containing an aromatic ring in the tail.

of the pterin moiety, may explain the near zero cross section observed for this derivative through the breaking of any π overlap that would aid in the transfer of electron density. The reduction in cross section as these derivatives move to their base form can be explained in a similar manner, in which the change in electronic structure of the pterin moiety, including the development of a formal negative charge on the oxygen, would reduce the ability of this moiety to accommodate charge from the tail. In contrast, the higher energy state (S_5 in the acid form; S_4 in the base form) is characterised by a π–π* transition isolated to the aromatic ring located in the tail which explains the observation that, while the cross sections of the states to change from the acid to base form, the state remains accessible across both forms.

3.4. Oxidised derivatives

The derivatives achieved through oxidation of the pterin moiety, shown in Fig. 3, present a significantly blue shifted spectra compared to structures in which the pterin moiety is left intact, with the additional feature of increased intensity in the shoulder region. The TPA spectra of these structures (Table 7) show a shared accessible state slightly red shifted in comparison to the lower energy peak of the OPA spectra. A second, TPA accessible, state can be seen for **MTHFG** at 5.76 eV with a cross sectional value of 22.40 GM; access to the **MTHFG** 4.74 eV S_1 state can be achieved with a cross sectional value of 12.80 GM.

In a similar manner to the pterins involving tails which contain an aromatic moiety, the oxidised derivatives studied here present a bright π–π* state that is shared across the derivatives (Table 7). This state can be found at S_4 for **FNA** (E = 4.95 eV; σ^{TP} = 19.5 GM) and S_3 for **MTHF** and **MTHFG** (E = 4.82 eV; σ^{TP} = 27.2 GM and E = 4.91 eV; σ^{TP} = 23.0 GM, respectively). However, while this is the only bright state on the TPA spectra of **FNA** and **MTHF** that overlaps with the lower band of the OPA spectra, this is not the case with **MTHFG**. The cyclisation between the tail and the oxidised pterin moiety results in the structure of **MTHFG** adopting a more planar geometry which, as seen with the acidic form of both PA_a and FA_a (Table 5), results in additional bright states. The first of these states is S_1 (E = 4.74 eV; σ^{TP} = 12.8 GM), which is characterised as a π–π* transition from a hole orbital with density on the substituted ring of the oxidised pterin moiety, the 5-membered ring linking it to the tail, and the aromatic ring of the tail itself, to

Table 5 State energies (eV) and two-photon cross sections (GM) of pterin derivatives with extended tails in their acidic form

	PA		FA		MFA	
State	E	σ^{TP}	E	σ^{TP}	E	σ^{TP}
1	3.87	51.100	3.84	60.600	3.58	0.078
2	3.95	0.040	3.95	0.027	4.02	0.086
3	4.22	9.930	4.22	10.200	4.20	0.977
4	4.69	6.830	4.67	0.987	4.54	0.825
5	4.85	41.900	4.82	55.700	4.74	23.100
6	4.89	1.090	4.86	13.900	4.81	5.770
7	4.90	6.360	4.89	0.944	4.89	0.012
8	4.99	0.197	4.99	0.268	4.99	2.800
9	5.09	10.000	5.08	12.900	5.09	1.680
10	5.43	0.000	5.25	3.320	5.23	0.950

Table 6 State energies (eV) and two-photon cross sections (GM) of pterin derivatives with extended tails in their base form

	PA		FA		MFA	
State	E	σ^{TP}	E	σ^{TP}	E	σ^{TP}
1	3.64	0.765	3.64	0.822	3.56	0.125
2	3.66	0.193	3.66	0.206	3.65	3.020
3	4.32	0.005	4.32	0.006	4.22	0.237
4	4.48	16.700	4.47	34.000	4.31	64.000
5	4.54	6.220	4.54	8.490	4.49	3.500
6	4.69	1.390	4.59	1.880	4.57	3.860
7	4.76	5.890	4.77	3.360	4.61	7.790
8	4.78	0.078	4.78	0.091	4.72	0.131
9	4.92	0.027	4.92	0.036	4.87	1.200
10	5.16	2.560	5.15	3.380	5.10	3.660

Table 7 State energies (eV) and two-photon cross sections (GM) of oxidised pterin derivatives

	FNA		MTHF		MTHFG	
State	E	σ^{TP}	E	σ^{TP}	E	σ^{TP}
1	4.73	9.220	4.73	5.680	4.74	12.800
2	4.84	0.575	4.74	6.310	4.76	3.330
3	4.88	3.020	4.82	27.200	4.91	23.000
4	4.95	19.500	5.02	1.240	4.92	0.570
5	5.21	2.900	5.25	4.190	5.09	4.870
6	5.24	1.730	5.26	5.340	5.17	7.310
7	5.27	1.600	5.28	3.100	5.25	1.790
8	5.51	0.374	5.74	0.498	5.76	22.400
9	5.60	4.390	5.86	3.130	5.82	3.310
10	5.88	1.340	5.94	3.750	5.85	0.028
11	5.92	0.175	6.00	6.640	5.97	0.173
12	6.01	1.030	6.02	0.012	6.05	0.159
13	6.01	0.011	6.06	0.113	6.11	0.782
14	6.07	0.079	6.13	1.090	6.18	16.400
15	6.12	23.200	6.16	2.370	6.27	4.120
16	6.16	7.360	6.22	7.850	6.33	1.830
17	6.25	10.100	6.33	2.870	6.36	0.262
18	6.29	1.010	6.36	0.084	6.41	1.180
19	6.34	7.400	6.47	6.050	6.44	2.210
20	6.46	5.200	6.53	4.100	6.52	9.670
21	6.46	2.300	6.57	2.280	6.53	4.410
22	6.52	12.600	6.57	6.940	6.61	1.450
23	6.61	0.817	6.68	18.900	6.63	1.160
24	6.68	2.290	6.71	5.680	6.73	2.400
25	6.73	4.490	6.73	2.980	6.78	27.200
26	6.75	2.490	6.76	41.100	6.80	4.940
27	6.78	13.200	6.81	9.400	6.82	4.260
28	6.84	0.972	6.86	4.900	6.83	2.830
29	6.86	1.300	6.92	1.280	6.86	0.421
30	6.92	0.757	6.95	2.460	6.90	12.000

a particle π* orbital isolated on the oxidised pterin moiety. The second of these states is S_8 (E = 5.76 eV; σ^{TP} = 22.4 GM) which is characterised by a charge transfer from a π hole orbital isolated on the oxidised pterin moiety to a particle π* orbital on the aromatic ring of the tail (Fig. 3; bottom); the charge transfer nature of this transition makes the high cross section associated to it dependent on the planarity of the geometry compared to the twisted geometry of **MTHF** in an analogous manner as seen when comparing the acid forms of $\mathbf{FA_a}$ and $\mathbf{MFA_a}$ (Table 5).

In addition to the TPA accessibility of the low energy shoulder of the OPA spectra (Fig. 10), all three structures studied also show significant accessibility for the high energy OPA peak. Each structure presents a constantly accessible π–π* state isolated to the tail such as that seen in S_5 of $\mathbf{FA_a}$ (Fig. 7); this state remains at ≈6.80 eV across the structures. In comparison, the second accessible state of this band more structurally specific; S_{22} of **FNA** (E = 6.52 eV; σ^{TP} = 12.6 GM) shows a π–π* isolated to the head in which the particle orbital presents significant Rydberg character, whereas S_{23} (E = 6.68 eV; σ^{TP} = 18.9 GM) in **MTHF** and S_{30} (E = 6.90 eV; σ^{TP} = 12.0 GM) in **MTHFG** present charge transfer from tail to head and π–π* character isolated to the head, respectively.

Of particular interest in the comparison of the OPA and TPA spectra is the emergence of TPA accessible states in both **FNA** and **MTHFG** which lie in the dark region between the OPA spectra (≈6.0 eV; Fig. 10) in the form of a charge transfer state in which density shifts from the pterin moiety to the aromatic ring of the tail; these states are S_{15} in **FNA** (E = 6.12 eV; σ^{TP} = 23.2 GM) and S_{14} in **MTHFG** (E = 6.18 eV; σ^{TP} = 16.4 GM). While these states present similar character to that of S_3 in **MTHF** (E = 4.82 eV; σ^{TP} = 27.2 GM), these states are not accessible in the OPA spectra.

The accessibility of these two states for **MTHFG** (S_1 & S_8) is a particularly promising find as, in comparison to the OPA spectra (Fig. 10) which shows minimal differentiation between **MTHFG** and **MTHF**, the TPA spectra does enable the differentiation of these structures. This presents a novel route for investigating the activity of the methylenetetrahydrofolate reductase enzyme (MTHFR)[85–87] which catalyses the reduction and decyclisation of **MTHFG** to **MTHF**, a cofactor in the conversion of homocysteine to methionine *via* the methionine synthase enzyme, a process vital for DNA reproduction as part of the cysteine cycle.[88,89]

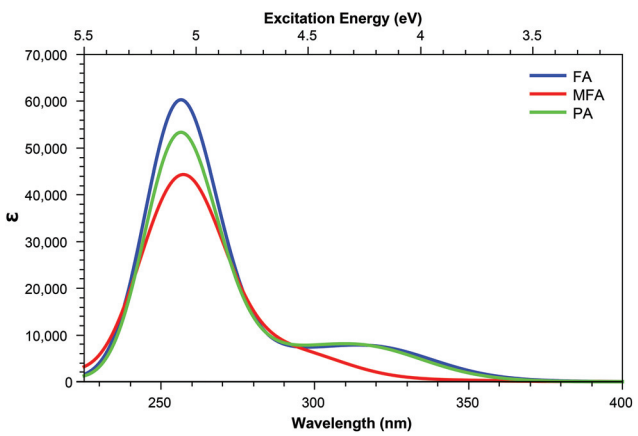

Fig. 8 One-photon absorption spectra of the acid form of pterin derivatives with extended tails.

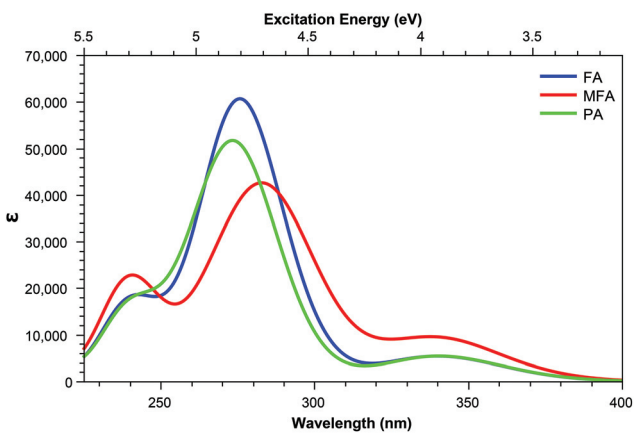

Fig. 9 One-photon absorption spectra of the base form of pterin derivatives with extended tails.

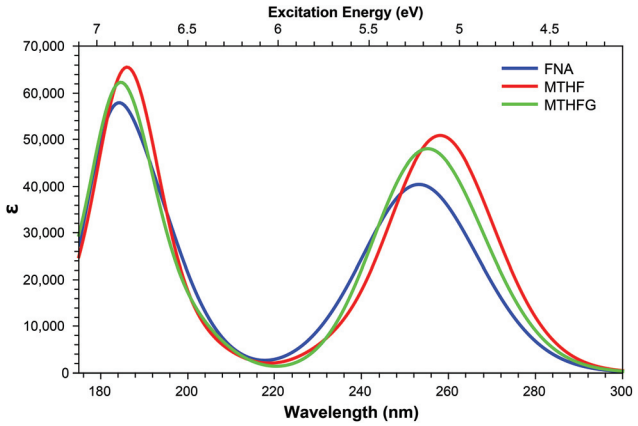

Fig. 10 One-photon absorption spectra of structures derived from modifications to the pterin moiety.

4. Conclusion and outlook

Analysis of the structures presented here reveals a trend in the accessibility of secondary states (defined here as those that are of significantly smaller cross sectional value than the dominant TPA peaks for a given structure); this trend shows that, while these states have a near zero value for a large number of states when looking to the small tail derivatives (Tables 2 and 4), the cross sectional values of these states increases with structural complexity. The derivatives containing an aromatic element in the tail (Tables 5 and 6) show an increased number of secondary states with a cross sectional value >1 GM while, when considering the oxidised derivatives (Table 7), the majority of secondary states present a >1 GM cross section.

Due to the lack of symmetry present throughout the pterin systems, the parity rules which act to limit the accessible states of symmetric systems do not apply to the structures studied here; this has the effect of, theoretically, rendering the entire singlet manifold assessable, with the cross section of a given state determined predominantly by the overlap of the particle and hole orbitals.

Across the pterin structures, TPA accessible states can be isolated into three different groups of π–π* transitions: those where both the hole and particle orbitals are located on the pterin moiety; those where both are orbitals are isolated to the tail; and those involving charge transfer from the tail to the pterin moiety. The later two types of transitions are only present in derivatives containing an aromatic ring in the tail; derivates without an aromatic ring present TPA accessible states that are depicted solely by transitions from various hole orbitals to the same particle orbital (with the exception of **FPT**, this particle orbital is shown to be the LUMO). The analysis of the TPA spectra, when compared to its OPA counterpart, has shown the potential for targetting specific derivatives despite the minimal qualitative variation evident in the OPA spectra; this is particularly relevant for $\mathbf{NPT_a}$, $\mathbf{BPT_b}$, and $\mathbf{HPT_b}$.

Of particular interest are the third category of states, those involving charge transfer from tail to pterin moiety where the nature of these states means that access to them is heavily dependent on the molecular geometry. This geometry dependence enables photochemical investigation of methylation and substitution events such as the conversion of **FA** to **MFA**, or the ring opening of **MTHFG** to form **MTHF**; the utilisation of TPA in these situations presents the possibility for structural differentiation that is not observable in the OPA spectra, due to the density of accessible states, potentially lending new insight into these biologically important processes.

Conflicts of interest

There are no conflicts to declare.

Acknowledgements

M. J. P. thanks the EPSRC for funding through Platform Grant EP/P001459/1 and Programme Grant EP/T021675, while T. M. thanks the The High End Computing facility at Lancaster University.

References

1 M. Vignoni, N. Walalawela, S. M. Bonesi, A. Greer and A. H. Thomas, *Mol. Pharm.*, 2018, **15**, 798.
2 A. Albert, *Biochem. J.*, 1953, **54**, 646.
3 C. Lorente and A. H. Thomas, *Acc. Chem. Res.*, 2006, **39**, 395.
4 H. Rokos, W. D. Beazlwy and K. U. Schallreuter, *Biochem. Biophys. Res. Commun.*, 2002, **292**, 805.
5 M. Pacileo, P. Cirillo, S. De Rosa, G. Ucci, G. Petrillo, S. Musto D'Amore, L. Sasso, P. Maietta, R. Spangnuolo and M. Chiariello, *Monaldi Arch. Chest Dis.*, 2007, **68**, 68.
6 A. Csordas, D. Fuchs, A. H. Frangieh, G. Reibnegger, B. Stähli, M. Cahenzly, F. Nietlispach, W. Maier, F. Maisano, R. K. Binder, C. Liebetreu, W. Kim, C. Hamm and T. F. Lüscher, *IJC Metab Endocr*, 2016, **10**, 7.
7 C. Murr, B. Widner, B. Wirleitner and D. Fuchs, *Curr. Drug Metab.*, 2002, **3**, 175.
8 C. A. Firth, A. D. Laing, S. K. Baird, J. Pearson and S. P. Gieseg, *Clin. Biochem.*, 2008, **41**, 1078.
9 R. L. Blakley, *The Biochemistry of Folic Acid*, North-Holland Publishing Co., 1969.
10 C. A. Nichol, G. K. Smith and D. S. Duch, *Annu. Rev. Biochem.*, 1985, **54**, 729.
11 J. M. Hevel and M. A. Marletta, *Biochemistry*, 1992, **31**, 7160.
12 D. Fuchs, A. Hausen, G. Reibnegger, E. R. Werner, M. P. Dierich and H. Wachter, *Immunol. Today*, 1988, **9**, 150.
13 C. Chandrashekar, K. Balaji, P. H. Vasudev, G. M. Panachiyil and T. Babu, *Int. J. Pediatr. Adolesc. Med.*, 2019, **6**, 151.
14 S. Geisler, S. D. Lytton, N. L. Toan, T. H. Nghia, N. M. Nam, H. V. Hung, N. T. Son, D. T. Anh, H. T. Tuyen, T. V. Tien,

D. Quyet, H. V. Tong, N. X. Hoan, L. H. Song, S. R. Pallerla, J. M. Gostner, D. Fuchs and T. P. Velavan, *Int. J. Infect. Dis.*, 2020, **91**, 162.

15 S. E. Dibakou, A. Souza, L. Boundenga, L. Givalois, S. Mercier-Delarue, F. Simon, F. Prugnolle, E. Huchard and M. J. E. Charpentier, *Int. J. Parasitol. Parasites Wildl.*, 2020, **11**, 198.

16 S. P. Gieseg, G. Baxter-Parker and A. Lindsay, *Antioxidants*, 2018, **7**, 80.

17 G. Reibnegger, *ChemistrySelect*, 2018, **3**, 10925.

18 P. Heelis, S. T. Kim, T. Okamura and A. Sancar, *J. Photochem. Photobiol., B*, 1993, **17**, 219.

19 J. L. Johnson, S. Hamm-Alvarez, G. Payne, G. B. Sancar, K. V. Rajagopalan and A. Sancar, *Proc. Natl. Acad. Sci. U. S. A.*, 1988, **85**, 2046.

20 J. E. Hearst, *Science*, 1995, **268**, 1858.

21 K. Ito and S. Kawanishi, *Biochemistry*, 1997, **36**, 1774.

22 S. Estébanez, A. H. Thomas and C. Lorente, *ChemPhysChem*, 2018, **19**, 300.

23 M. P. Serrano, M. Vignoni, C. Lorente, P. Vicendo, E. Oliveros and A. H. Thomas, *Free Radicals Biol. Med.*, 2016, **96**, 418.

24 M. P. Serrano, C. D. Borsarelli and A. H. Thomas, *Photochem. Photobiol.*, 2013, **89**, 1456.

25 C. Lorente, A. H. Thomas, L. S. Villata, D. Hozbor, A. Lagares and A. L. Capparelli, *Pteridines*, 2000, **11**, 100.

26 S. Y. Egorov, A. A. Krasnovsky Jr., M. E. Bashtanov, E. A. Mironov, T. A. Lyudnikova and M. S. Kritsky, *Biochemistry*, 1999, **64**, 1325.

27 E. Oliveros, M. L. Dántola, M. Vignoni, A. H. Thomas and C. Lorente, *Pure Appl. Chem.*, 2011, **83**, 801.

28 A. A. Buglak, T. A. Telegina, E. A. Vorotelyak and A. I. Kononov, *J. Photochem. Photobiol., A*, 2019, **372**, 254.

29 A. H. Thomas, C. Lorente, A. L. Capparelli, C. G. Martínez, A. M. Braun and E. Oliveros, *J. Photochem. Photobiol., A*, 2019, **372**, 254.

30 J. W. Ledbetter Jr., W. Pfleiderer and J. H. Freisheim, *Photochem. Photobiol.*, 1995, **62**, 71.

31 K. V. Neverov, E. A. Mironov, T. A. Lyudnikova, A. A. Krasnovsky and M. S. Kritsky, *Biochemistry*, 1996, **61**, 1149.

32 A. H. Thomas, C. Lorente, A. L. Capparelli, M. R. Pokhrel, A. M. Braun and E. Oliveros, *Photochem. Photobiol. Sci.*, 2002, **1**, 421.

33 J. R. Mourant, J. Frever, A. Hielscher, A. Fick, D. Shen and T. Johnson, *Appl. Opt.*, 1998, **37**, 3586.

34 J. R. Mourant, M. Canpolat, C. Brocker, O. Esponda-Ramos, T. Johnson, A. Matanock, K. Stetter and J. Freyer, *J. Biomed. Opt.*, 2000, **5**, 131.

35 S. Stolik, J. A. Delgado, A. Perez and L. Anasagasti, *J. Photochem. Photobiol., B*, 2000, **57**, 90.

36 G. G. Kramarenko, S. G. Hummel, S. M. Martin and G. R. Buetner, *Photochem. Photobiol.*, 2006, **82**, 1634.

37 D. Havrylyuk, D. K. Heidary, L. Nease, S. Parkin and E. C. Glazer, *Eur. J. Inorg. Chem.*, 2017, **12**, 1687.

38 E. C. Glazer, *Photochem. Photobiol.*, 2017, **12**, 1326.

39 E. Skovsen, J. W. Snyder, J. D. Lambert and P. R. Ogilby, *J. Phys. Chem. B*, 2005, **109**, 8570.

40 S. Kim, T. Tachikawa, M. Fujitsuka and T. Majima, *J. Am. Chem. Soc.*, 2014, **136**, 11707.

41 T. L. To, K. F. Medzihradszky, A. L. Burlingame, W. F. DeGrado, H. Jo and X. Shu, *Bioorg. Med. Chem. Lett.*, 2016, **26**, 3359.

42 C. Ash, M. Dubec, K. Donne and T. Bashford, *Lasers Med. Sci.*, 2017, **32**, 1909.

43 H. Zhang, D. Salo, D. M. Kim, S. Komarov, Y. Tai and M. Y. Berezin, *J. Biomed. Opt.*, 2016, **21**, 126006.

44 K. Datta, N. P. Johnson, G. Villani, A. H. Marcus and P. H. von Hippel, *Nucleic Acids Res.*, 2012, **40**, 1191.

45 K. Yang, S. Matsika and R. J. Stanley, *J. Phys. Chem. B*, 2007, **111**, 10615.

46 M. L. Dántola, M. Vignoni, C. González, C. Lorente, P. Vicendo, E. Oliveros and A. H. Thomas, *Free Radicals Biol. Med.*, 2010, **49**, 1014.

47 J. Arnberg, A. Jiménez-Banzo, M. J. Patersin, S. Nonell, J. I. Borrell, O. Christiansen and P. R. Ogilby, *J. Am. Chem. Soc.*, 2007, **129**, 5188.

48 L. T. Bergendahl and M. J. Paterson, *J. Phys. Chem. B*, 2012, **116**, 11818.

49 A. Graczyk, J. M. Žurek and M. J. Paterson, *Photochem. Photobiol. Sci.*, 2014, **13**, 103.

50 S. E. Greenough, M. D. Hornbury, N. A. Smith, P. J. Sadler and M. J. Paterson, *Photochem. Photobiol. Sci.*, 2014, **13**, 103.

51 P. Zhang, C. K. C. Chiu, H. Huang, Y. P. Y. Lam, A. Habtemariam, T. Malcomson, M. J. Paterson, G. J. Clarkson, P. B. O'Connor, H. Chao and P. J. Sadler, *Angew. Chem., Int. Ed.*, 2017, **56**, 14898.

52 H. Huang, S. Banerjee, K. Qiu, O. Blacque, T. Malcomson, M. J. Paterson, G. J. Clarkson, M. Staniforth, V. G. Stravos, G. Gasser, H. Chao and P. J. Sadler, *Nat. Chem.*, 2019, **11**, 1041.

53 T. Malcomson, R. McKinlay and M. J. Paterson, *ChemPhotoChem*, 2019, **3**, 825.

54 M. J. Frisch, G. W. Trucks, H. B. Schlegel, G. E. Scuseria, M. A. Robb, J. R. Cheeseman, G. Scalmani, V. Barone, G. A. Petersson, H. Nakatsuji, X. Li, M. Caricato, A. V. Marenich, J. Bloino, B. G. Janesko, R. Gomperts, B. Mennucci, H. P. Hratchian, J. V. Ortiz, A. F. Izmaylov, J. L. Sonnenberg, D. Williams-Young, F. Ding, F. Lipparini, F. Egidi, J. Goings, B. Peng, A. Petrone, T. Henderson, D. Ranasinghe, V. G. Zakrzewski, J. Gao, N. Rega, G. Zheng, W. Liang, M. Hada, M. Ehara, K. Toyota, R. Fukuda, J. Hasegawa, M. Ishida, T. Nakajima, Y. Honda, O. Kitao, H. Nakai, T. Vreven, K. Throssell, J. A. Montgomery Jr., J. E. Peralta, F. Ogliaro, M. J. Bearpark, J. J. Heyd, E. N. Brothers, K. N. Kudin, V. N. Staroverov, T. A. Keith, R. Kobayashi, J. Normand, K. Raghavachari, A. P. Rendell, J. C. Burant, S. S. Iyengar, J. Tomasi, M. Cossi, J. M. Millam, M. Klene, C. Adamo, R. Cammi, J. W. Ochterski, R. L. Martin, K. Morokuma, O. Farkas, J. B. Foresman and D. J. Fox, *Gaussian16*, Gaussian Inc., Wallingford CT, 2016.

55 R. Dennington, T. A. Keith and J. M. Millam, GaussView Version 6, Semichem Inc., Shawnee Mission KS, 2016.

56 B. Miehlich, A. Savin, H. Stoll and H. Preuss, *Chem. Phys. Lett.*, 1989, **157**, 200.
57 C. Lee, W. Yang and R. G. Parr, *Phys. Rev.*, 1988, **37**, 785.
58 A. D. Becke, *J. Chem. Phys.*, 1993, **98**, 1372.
59 A. D. Becke, *Phys. Rev.*, 1988, **38**, 3098.
60 R. Krishnan, J. S. Binkley, R. Seeger and J. A. Pople, *J. Chem. Phys.*, 1980, **72**, 650.
61 S. Grimme, S. Ehrlich and L. Goerigk, *J. Comput. Chem.*, 2011, **32**, 1456.
62 A. D. Becke and E. R. Johnson, *J. Chem. Phys.*, 2007, **127**, 154108.
63 A. D. Becke and E. R. Johnson, *J. Chem. Phys.*, 2005, **122**, 154104.
64 A. D. Becke and E. R. Johnson, *J. Chem. Phys.*, 2005, **123**, 154101.
65 A. D. Becke and E. R. Johnson, *J. Chem. Phys.*, 2006, **124**, 174104.
66 R. Krishnan, J. S. Binkley, R. Seeger and J. A. Pople, *J. Chem. Phys.*, 1980, **72**, 650.
67 P. Jaramillo, K. Coutinho and S. Canuto, *Int. J. Quantum Chem.*, 2010, **110**, 2371.
68 G. Reibnegger, *Pteridines*, 2015, **26**, 135.
69 M. Soniat and C. B. Martin, *Pteridines*, 2008, **19**, 120.
70 M. Soniat and C. B. Martin, *Pteridines*, 2009, **20**, 124.
71 M. Soniat and C. B. Martin, *Pteridines*, 2015, **26**, 13.
72 T. Yanai, D. P. Tew and N. C. Handy, *Chem. Phys. Lett.*, 2004, **393**, 51.
73 A. D. Becke, *Phys. Rev. A: At., Mol., Opt. Phys.*, 1999, **38**, 3098.
74 J. P. Perdew, *Phys. Rev. B: Condens. Matter Mater. Phys.*, 1986, **33**, 8822.
75 C. Adamo and V. Barone, *J. Chem. Phys.*, 1999, **110**, 6158.
76 T. H. Dunning, *J. Chem. Phys.*, 1989, **90**, 1007–1023.
77 M. Baibarac, I. Smaranda, A. Nila and C. Serbschi, *Sci. Rep.*, 2019, **9**, 14278.
78 A. Ali, M. I. Rafiq, Z. Zhang, J. Cao, R. Geng, B. Zhou and W. Tang, *Phys. Chem. Chem. Phys.*, 2020, **22**, 7864.
79 D. Jacquemin, V. Wathelet, E. A. Perpète and C. Adamo, *J. Chem. Theory Comput.*, 2009, **5**, 2420.
80 M. J. Patersin, O. Christiansen, F. Pawłowski, P. Jørgensen, C. Hättig, T. Helgaker and P. J. Sałek, *Chem. Phys.*, 2006, **124**, 054322.
81 J. Arnberg, M. J. Paterson, C. B. Nielsen, M. Jørgensen, O. Christiansen and P. R. Ogilby, *J. Phys. Chem. A*, 2007, **111**, 5756.
82 M. Johnsen, M. J. Paterson, F. Arnberg, O. Christiansen, C. B. Nielsen, M. Jørgensen and P. R. Ogilby, *Phys. Chem. Chem. Phys.*, 2008, **10**, 1177.
83 L. T. Bergendahl and M. J. Paterson, *Chem. Commun.*, 2012, **48**, 1544.
84 K. Aidas, C. Angeli, K. L. Bak, V. Bakken, R. Bast, L. Boman, O. Christiansen, R. Cimiraglia, S. Coriani, P. Dahle, E. K. Dalskov, U. Ekström, T. Enevoldsen, J. J. Eriksen, P. Ettenhuber, B. Fernández, L. Ferrighi, H. Fliegl, L. Frediani, K. Hald, A. Halkier, C. Hátig, H. Heiberg, T. Helgaker, A. C. Hennum, H. Hettema, E. Hjertenæs, S. H. Høst, I.-M. Høyvik, M. F. Iozzi, B. Jansik, H. J. A. Jensen, D. Jonsson, P. Jørgensen, J. Kauczor, S. Kirpekar, T. Kjærgaard, W. Klooper, S. Knecht, R. Kobayashi, H. Koch, J. Kongsted, A. Krapp, K. Kristensen, A. Ligabue, O. B. Lutnæs, J. I. Melo, K. V. Mikkelsen, R. H. Myhre, C. Neiss, C. B. Nielsen, P. Norman, J. Olsen, J. M. H. Olsen, A. Osted, M. J. Packer, F. Pawlowski, T. B. Pedersen, P. F. Provasi, S. Reine, Z. Rinkevicius, T. A. Ruden, K. Ruud, V. Rybkin, P. Salek, C. C. M. Samson, A. Sánchez de Merás, T. Saue, S. P. A. Sauer, B. Schimmelpfennig, K. Sneskov, A. H. Steindal, K. O. Sylvester-Hvid, P. R. Taylor, A. M. Teale, E. I. Tellgren, D. P. Tew, A. J. Thorvaldsen, L. Thøgersen, O. Vahtras, M. A. Watson, D. J. D. Wilson, M. Ziolkowski and H. Ågren, *Wiley Interdiscip. Rev.: Comput. Mol. Sci.*, 2014, **4**, 269.
85 E. E. Trimmer, *Curr. Pharm. Des.*, 2013, **19**, 2574.
86 R. Reilly, H. McNulty, K. Pentieva, J. J. Strain and M. Ward, *Proc. Nutr. Soc.*, 2014, **73**, 47.
87 R. P. Ojha and J. G. Gurney, *Leuk. Lymphoma*, 2014, **55**, 67.
88 V. Forster, F. van Delft, S. Baird, S. Mair, R. Skinner and C. Halsey, *Cancer Chemother. Pharmacol.*, 2016, **78**, 1093.
89 A. Banjac, T. Perisic, H. Sato, A. Seiler, S. Bannai, N. Weiss, P. Kölle, K. Tschoep, R. D. Issels, P. T. Daniel, M. Conrad and G. W. Bornkamm, *Oncogene*, 2008, **27**, 1618.